Confinement Induced Plastic Crystal-to-Crystal Transitions in Rodlike Particles with Long-Ranged Repulsion

Bing Liu,[*] Thijs H. Besseling, Alfons van Blaaderen, and Arnout Imhof[†]

Soft Condensed Matter, Debye Institute for Nanomaterials Science, Utrecht University,
Princetonplein 5, 3584 CC Utrecht, Netherlands

Colloidal particles in geometrical confinement display a complex variety of packing structures different from their three-dimensional (3D) bulk counterpart. Here, we confined charged rodlike colloids with long-ranged repulsions to a thin wedge-shaped cell and show, by quantitative 3D confocal microscopy, that not only their positional but also their orientational order depends sensitively upon the slit width. Synchronized with transitions in lattice symmetry and number of layers confinement induces plastic crystal-to-crystal transitions. A model analysis suggests that this complex sequence of more or less rotationally ordered states originates from the subtle competition between the electrostatic repulsion of a rod with the wall and with its neighbors.

                                                                    PACS numbers: 82.70.Dd, 64.75.Yz

When a colloidal suspension is confined to a quasi-two-dimensional geometry, many fascinating crystal structures appear due to the partial restriction of translational degrees of freedom in the third dimension [1–3]. In the case of particles interacting with a hard potential the structure greatly depends on their packing efficiency in the confined geometry. One of the first studies in this limit was performed by Pieranski *et al.*, who used nearly hard spherical colloids confined in a wedge-shaped cell. At increasing slit width they found a sequence of transitions that can be represented as: $n\triangle \rightarrow (n+1)\square \rightarrow (n+1)\triangle$, where n denotes the number of crystal layers and $\triangle$ and $\square$ denote layers with hexagonal and square symmetry, respectively [4]. More detailed investigations since then disclosed that many intermediate phases exist, such as a buckling phase in between $1\triangle \rightarrow 2\square$, a rhombic phase in between $n\square \rightarrow n\triangle$, and prismatic, hexagonal close packing (hcp)-like, hcp(100), hcp⊥, and pre-square phases in between $n\triangle \rightarrow (n+1)\square$ [3,5–7]. All these structures have been verified by computer simulations [8–13], and the consistency between experiments and simulations gives us confidence in our understanding of the nature of the transitions for hard spheres.

Fewer intermediate phases are found for charged spheres, which interact via long-ranged electrostatic interactions, both with each other and with the walls [14–17]. Using colloids with $\kappa a = 0.79$ and 0.37 (where κ is the inverse Debye screening length characterizing the range of the repulsive interactions, and a is the particle radius) we found a phase sequence very similar to Ref. [16]: $1\triangle \rightarrow 2\square \rightarrow 2R \rightarrow 2\triangle \rightarrow 3\square \rightarrow 3R \rightarrow 3\triangle \rightarrow 4\square \rightarrow 4R \rightarrow 4\triangle$ (R denotes a rhombic phase) [17]. These observations imply that long-ranged electrostatic interactions play an important additional role in the packing of charged particles.

The packing behavior of shape anisotropic particles has also begun to be explored. For nearly hard dimer-shaped particles so-called "side" and "out-of-plane" structures were reported [18,19]. This leads to questions about the effect of confinement on particle orientational order in a system where this effect can be separated from packing-dominated changes in the lattice symmetry. Therefore, we consider a system of rod-shaped particles with long-ranged electrostatic repulsion and present the unexpected observation that confinement induces plastic crystal-to-crystal transitions in the rod orientations that are synchronized with transitions in the lattice symmetry and the number of crystalline layers. Recent advances in quantitative three-dimensional (3D) real space analysis have made it possible to measure both positions and orientations of rodlike particles with high accuracy and sufficient temporal resolution [20–23]. In a 3D bulk phase at the same packing fraction of $\phi = 0.0026$ the rods were found to form a body centered cubic (bcc) plastic crystal and to rotate freely in all directions [22]. Confined between two parallel plates, however, their rotational freedom in the z direction (perpendicular to the walls) was now found to be completely or partially restricted as a function of the wall separation.

The charged rods we employed were made of fluorescently labeled silica [24,25] and had a length of 2.29 μm and a diameter of 0.60 μm (see Supplemental Material [26]). They were made hydrophobic by grafting with alkyl chains (C_{18}) and dispersed in the almost index-matching solvent cyclohexyl chloride. In this solvent of dielectric constant $\varepsilon = 7.6$ the range of electrostatic repulsions is increased and van der Waals forces minimized. The solvent was partially deionized so as to have a controlled conductivity of 180 pS/cm, corresponding to a screening length $\kappa^{-1} = 1.2$ μm. This value is comparable to the size of the

rods, so that the anisotropy of the rod-rod interaction potential is significantly less than the shape anisotropy. The surface potential (taken the same as the zeta potential) on the silica rods was estimated to be 50 mV, in accordance with that of silica spheres under the same conditions. We used a wedge-shaped cell with a very small wedge angle ($< 10^{-3}$ rad) for our experimental observations using confocal microscopy (see Supplemental Material [26] for a schematic illustration). The difference in slit width d across the imaging area of $79.4 \times 79.4 \ \mu m^2$ was $0.072 \ \mu m$. Since this is much smaller than the typical interrod distance of $> 5 \ \mu m$ the plates may be regarded as parallel. The cell surfaces were coated with a silica layer (~ 40 nm, identical to that of the rods) [35] and then grafted with alkyl chains (C_{18}), to impart a similar surface chemistry as the rods. A maximum wall separation of $50 \ \mu m$ allowed us to observe crystals of up to 4 layers.

An overview of the observed crystal symmetries is shown in Fig. 1. The quality of the crystals formed can be seen in the movies in the Supplemental Material [26]. The sequence of the transitions observed for our long-ranged repulsive rod systems can also be summarized as $1\triangle \rightarrow 2\square \rightarrow 2R \rightarrow 2\triangle \rightarrow 3\square \rightarrow 3R \rightarrow 3\triangle \rightarrow 4\square \rightarrow 4R \rightarrow 4\triangle$, with an increase of the slit width d from 8.8 μm to 42.0 μm. This sequence is the same as the one we obtained for charged spheres at a similar screening length [17]. Apparently, it is due to the long range of the

repulsion, which gives the rods an effective aspect ratio of only 1.3, that the rods showed the same lattice sequence as that of long-range repulsive spheres, in accordance with the bcc bulk plastic crystal phase with (almost) free rotations of the rods on the lattice. In the bilayer region the two neighboring layers in the square, rhombic, and triangular phases showed staggered positioning, with the projected position of the particle in one layer situated in the geometric center of a primitive unit cell of the other. Moreover, we observed a unique rhombic phase with an almost perfect hexagonal lattice that makes it different from two known rhombic phases in a Yukawa system [15], and has been first observed in a system of spherical particles [17]. For more than two layers ($n > 2$), $n\square$ and nR showed $ABAB$ stacking. For $n\triangle$, we observed a mixture of ABC (face centered cubic, fcc) and ABA hcp stacking. Full details of the crystal structures are provided in the Supplemental material [26]. We did not observe a buckling phase, nor the prismatic, hcp-like, hcp(100), and hcp⊥ phases observed for hard spheres [3,5–7,17]. Their absence is most likely due to the increased softness of the interaction, which causes a weaker confinement and a different role of packing entropy in the phase behavior, which is also apparent from the bulk bcc phase being different from close packed structures observed for bulk hard spheres. The interlayer spacing also showed a dependence on slit width. Extracting the relative positions of each crystal layer with respect to the wall yielded the spacing at which the transitions take place [Fig. 2(a)]. In the ranges 17.7–21.5 μm and 33.5–36.7 μm there was no change in the lattice, so no data were collected there. For the rhombic point at 34.0 μm the layer positions were accidentally not measured. A stronger repulsion between the walls and the layers than that between layers can be inferred from the larger distance with the walls. The almost symmetrical layer positioning is evidence that gravity is negligible at this small number of layers. From Fig. 2(a), three lattice transitions were clearly visible: (1) from $n\triangle$ to $n + 1\square$, (2) from $n\square$ to nR, and (3) from nR to $n\triangle$.

Details of the transitions were investigated by calculating the 2D bond order parameters ψ_4 and ψ_6 [26] and 2D pair correlation functions $g(r)$ from the averaged positions of the centers of mass of the rods averaged over 81.8 s. Alternating jumps in ψ_4 and ψ_6 reflect the structural transitions, as the square lattice has $\psi_4 \sim 1$ and $\psi_6 \sim 0$, whereas the hexagonal lattice has $\psi_6 \sim 1$ and $\psi_4 \sim 0$ [Fig. 2(a)]. The rhombic lattice has intermediate values, as expected. In the monolayer region, all $g(r)'$s show similar peaks and thus the same distance distributions [26]. It should be noted that the interrod distance slowly increased with d for the smallest gap widths. However, for $d > 10.2 \ \mu m$ this phenomenon was not observed. At small wall separations, relatively more counterions from the walls could result in a smaller screening length. In the bilayer region, transitions from square to rhombic to hexagonal packing are clearly visible when comparing the
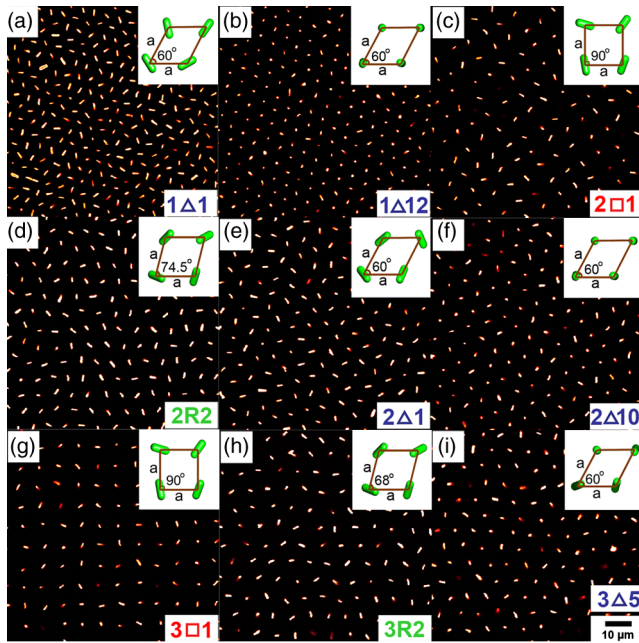

FIG. 1 (color online). Crystalline structures formed by charged rods in confinement. Slit widths are (a) 8.84 μm, (b) 14.89 μm, (c) 15.13 μm, (d) 16.91 μm, (e) 17.68 μm, (f) 24.04 μm, (g) 24.44 μm, (h) 26.99 μm, and (i) 30.56 μm. Insets show the lattice parameters. The 3-digit symbols characterizing each structure consist of the number of layers, lattice symmetry, and an index number. The uncertainty in angle measurement is estimated to be $\pm 1°$. The scale bar applies to Figs (a)–(i).
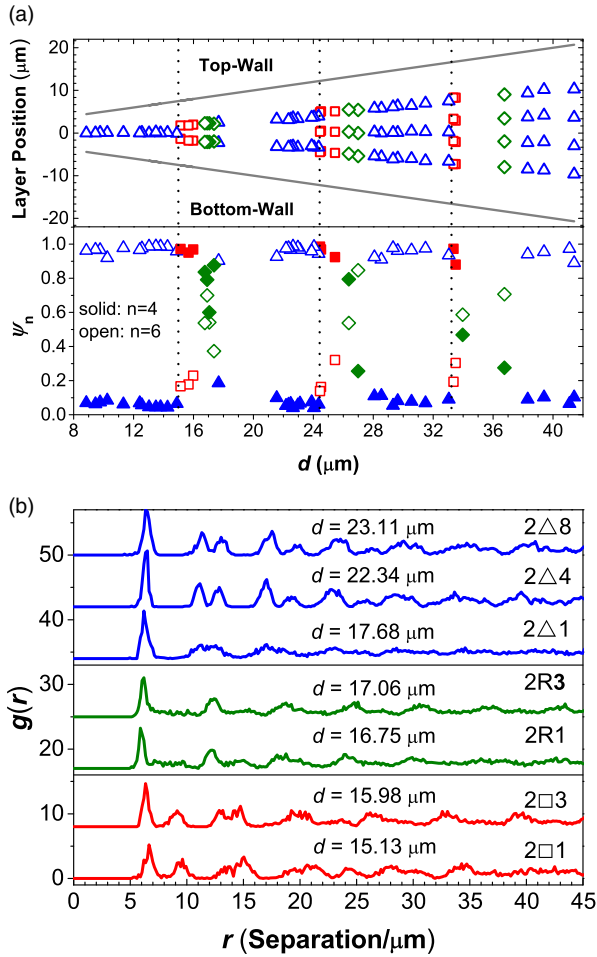
FIG. 2 (color online). Transitions in crystal lattice versus slit width d. (a) Crystal layer positions relative to the walls and 2D bond orientational order parameters ψ_4 and ψ_6. (b) 2D Pair correlation functions $g(r)$ in the bilayer region. $\triangle$, $\diamond$, and $\square$ denote layers with hexagonal, rhombic, and square symmetry, respectively.

FIG. 3 (color online). Orientational probability density functions (PDFs) and correlation functions. (a),(b) The distribution of the z component of rods' orientations u_z in the monolayer (a) and bilayer (b) region. S is the corresponding value of the orientational order parameter. Insets show trajectories that the orientation vector of a single rod traces out on the unit sphere. (c) Spatial orientational correlation function [$g_2(r)$, black, left axis] and positional pair correlation function [$g(r)$, brown, right axis] of rods for sample 1△1. (d) Time-dependent orientational autocorrelation functions $C_2(t)$ of rods in the monolayer region. Bars indicate the statistical standard error. Symbols $\triangle$, $\diamond$, and $\square$ denote layers with hexagonal, rhombic, and square symmetry, respectively.

positions of the peaks in $g(r)$ [Fig. 2(b)]. Similar transitions were observed in the trilayer and tetralayer regions [26].

We now describe the effects of wall separation on the orientational order and dynamics, which are surprisingly subtle (Fig. 3). We first calculated the probability density function (PDF) of the orientations of the rods' unit vectors **u** extracted from time series of images in x-y-z-t scanning mode [23]. Since a rod's tips cannot be distinguished due to symmetry we arbitrarily assigned the vector **u** to one of its tips and tracked it for the duration of the measurement. In all cases, regardless of d, the rods were found to explore orientations in the $x - y$ plane (the plane of the walls) with nearly equal probability [26]. Out-of-plane rotation, however, was much more restricted and depended strongly on d: In the monolayer region, at the smallest d of 8.8 μm the fairly narrow distribution of u_z indicates that the rods rotated mainly in the x-y plane [Fig. 3(a)]. This strongly restricted rotational motion is exemplified by the trajectory of a single rod and quantified by the orientational order parameter $S = \langle 3\cos^2\theta - 1 \rangle/2 = -0.47$ ($S = -0.5$ for
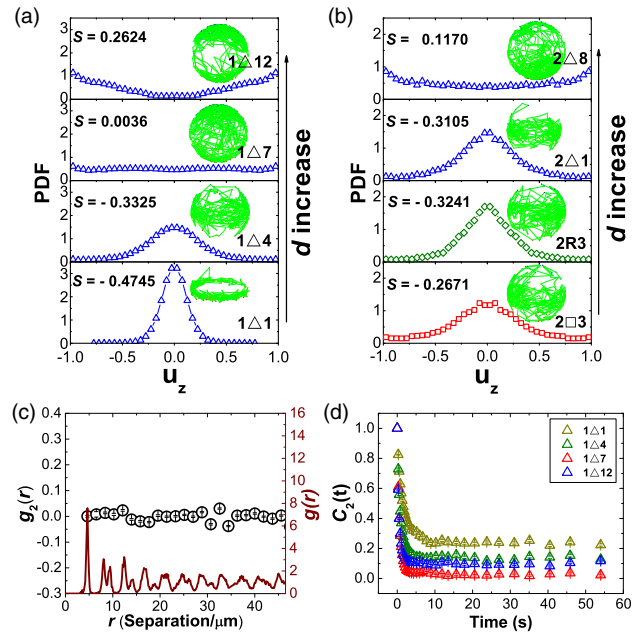
rods perfectly perpendicular to the z axis, $S = 0$ for random orientations, and $S = 1$ for perfect alignment with the z axis). The orientational spatial correlation function $g_2(r) = \langle \cos 2(\theta_i - \theta_j) \rangle$ [36] shows that the orientations of neighboring rods were uncorrelated [Fig. 3(c)]. The time-dependent orientational autocorrelation function $C_2(t) = \frac{1}{2}\langle (1/N)\sum_{i=1}^{N} 3[\mathbf{u}_i(0) \cdot \mathbf{u}_i(t)]^2 - 1 \rangle$ shows that the rods need only a few seconds to explore all orientations available to them [Fig. 3(d)]. However, the long-time value of this autocorrelation function is around 0.23. This is close to the 0.25 expected for a unit vector rotating in a two-dimensional subspace, suggesting that the rods have no strong rotational restriction in the x-y plane but hardly explore out-of-plane orientations.

With increasing d, the rods gradually took on more out-of-plane orientations [Fig. 3(a)]. Interestingly, an almost uniform distribution was found at $d = 12.6$ μm. This lack of preferred orientation is exemplified by the near-zero value of S ($= 0.0036$) and is clearly seen in the trajectory of a single rod, which almost uniformly covers the unit sphere. The almost zero long-time value of $C_2(t)$ of 0.03 also shows that the rotation of the rods was unrestricted [Fig. 3(d)]. These results indicate that the rods form a

monolayered plastic crystal with full 3D rotations for this interplate distance. Clearly, gravity hardly affects the rods' orientations, as an almost zero potential energy difference is incurred during the rotation of a rod confined to a lattice position. Surprisingly, for still wider slits (13.8 $\mu m < d < 15.0\ \mu m$) orientations became more restricted again, but this time to a direction perpendicular rather than parallel to the walls. That the long-time value of $C_2(t)$ is still almost zero [Fig. 3(d)] is attributed to the fact that the rods still occasionally flipped by 180 degrees, as is seen in the trajectory shown in Fig. 3(a). This sequence of events implies that, as far as we can determine, a continuous transition from a plastic crystal to a crystal took place. As far as we know, such a transition in the rotational behavior has not been observed in bulk phases, except when an external electric field was used [22]. Lee *et al.* reported a similar monolayered crystal but composed of dumbbell particles with a nearly hard potential oriented perpendicular to the wall [18]. Our results for rods with a very long-ranged repulsion now show that a confinement induced transition in the rotations of rods exists independently of a packing induced transition.

In the bilayer region, qualitatively similar, but less pronounced, changes in the orientational distribution functions were found. From 2□ to the early stages of 2△, the rods showed preferred orientation in the *x-y* plane [Fig. 3(b)]. Compared to the monolayer region, insertion of the second layer weakened the orienting effect of the confinement [compare the bottom curves in Figs. 3(a) and 3(b)]. The long-time decay of $C_2(t)$ shows that a smaller slit width always produced stronger confinement, which is particularly obvious when comparing the rods on lattices with the same symmetry. Just before entering the trilayer region, rods predominantly oriented perpendicular to the walls again [Fig. 3(b)] [26]. Compared to the monolayer region, this transition in rotational behavior weakened with an increasing number of crystal layers, although it was still discernible even at four layers (see Supplemental Material for details [26]).

Because of the long-range repulsive forces and weak orientational correlation between the rods, the sequence of lattice transitions observed is well approximated by recent theories and simulations for spheres [8–13,16]. However, the nature of the preferred orientations of rods in this quasi-2D confinement was found to be a subtle competition between repulsive rod-wall interactions, which favor the rods to be parallel to the wall, and repulsive rod-rod interactions, which favor the rods to be parallel to each other and perpendicular to the wall [26]. To see whether such a competition can indeed explain our observations we calculated the interaction energy of a rod with its neighbors and with the walls. Both energies were obtained using the Yukawa segment model [37–39], which divides the rod into a number of equal segments that each interact via pairwise additive point Yukawa interactions. A perfectly ordered hexagonal layer was assumed, with the experimentally measured lattice parameter and only interactions with first
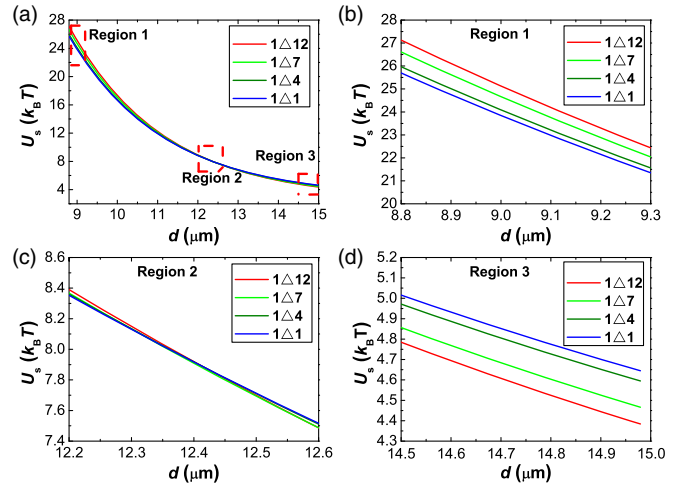

FIG. 4 (color online).   Average potential energy U_s of a rod in a one-layer hexagonal lattice confined to a slit as a function of slit width d. (a) Comparison of U_s between rods with different orientational distributions as measured on the systems indicated. (b)–(d) Close-ups of regions 1 (b), 2 (c), and 3 (d).

neighbors and the walls were included. The interaction energy was calculated as a function of rod orientation and then averaged over the experimentally measured orientation distribution for a range of slit widths in which changes in these distributions were observed. Because every rod is in the same surroundings, we only need the average repulsive energy of a single rod, denoted $U_s = U_{\text{tot}}/N$. Full calculation details are included in the Supplemental Material [26]. Figure 4 shows U_s as a function of d for samples 1△1, 1△4, 1△7, and 1△12. The curves showed a crossover: At small d [region 1, Fig. 4(b)], sample 1△1, with rods restricted to lie in the *x-y* plane. At large d [region 3, Fig. 4(d)], the lowest energy is now found for sample 1△12 with rods oriented mainly perpendicular to the walls. Around the crossover [region 2, Fig. 4(c)], the potential energies are close; thus, the rods are predicted to take on all orientations with equal probability. This sequence precisely reproduces the experimental one and is of the correct order of magnitude ($\sim k_B T$). A calculation for the bilayer region shows a similar result (see Supplemental Material [26]). This makes us confident that, despite the relatively strong assumptions made, the calculation of the interaction energies captures the most important effects.

In conclusion, both the positional and the orientational order of long-ranged repulsive rodlike colloids depend sensitively on the separation of confining charged walls. The positional order mirrors that observed for long-range repulsive spheres. However, rod orientations were strongly influenced by the presence of the walls despite the fact that interparticle distances were large enough to allow free rotation in bulk. While the rods oriented parallel to the walls at small separations they first became more randomly oriented, and finally assumed a perpendicular orientation when the separation was increased. This sequence repeated itself each time the wall separation became large enough to

accommodate an additional crystal layer, but in a less pronounced manner, until finally only a uniform orientation distribution was found in bulk. This high sensitivity offers opportunities to control particle orientations, while keeping them on a lattice, simply by controlling the slit width, and possibly also provides a new pathway to achieve vertical alignment of colloidal nanorods [40–42]. A plastic crystal of rods oriented in a gradient also has potential for photonic applications due to the anisotropic scattering of rods. More specifically, we have recently succeeded in creating plastic crystals of gold nanorods for which the anisotropic longitudinal and transverse plasmonic response are important for photonic applications [43]. We expect these transitions to be observable for particles with sizes over the entire colloidal range by using appropriate confinement. In principle, similar transitions in the rotational degrees of freedom should not be limited to rodlike particles, but be achievable for other anisotropic shapes as well.

---

[*]b.liu@uu.nl
[†]a.imhof@uu.nl

[1] C. Bechinger, Curr. Opin. Colloid Interface Sci. **7**, 204 (2002).
[2] H. Löwen, J. Phys. Condens. Matter **21**, 474203 (2009).
[3] F. Ramiro-Manzano, E. Bonet, I. Rodriguez, and F. Meseguer, Soft Matter **5**, 4279 (2009).
[4] P. Pieranski, L. Strzelecki, and B. Pansu, Phys. Rev. Lett. **50**, 900 (1983).
[5] S. Neser, C. Bechinger, P. Leiderer, and T. Palberg, Phys. Rev. Lett. **79**, 2348 (1997).
[6] A. B. Fontecha, T. Palberg, and H. J. Schöpe, Phys. Rev. E **76**, 050402 (2007).
[7] F. Ramiro-Manzano, E. Bonet, I. Rodriguez, and F. Meseguer, Phys. Rev. E **76**, 050401 (2007).
[8] E. C. Oğuz, M. Marechal, F. Ramiro-Manzano, I. Rodriguez, R. Messina, F. J. Meseguer, and H. Löwen, Phys. Rev. Lett. **109**, 218301 (2012).
[9] M. Schmidt and H. Löwen, Phys. Rev. Lett. **76**, 4552 (1996).
[10] M. Schmidt and H. Löwen, Phys. Rev. E **55**, 7228 (1997).
[11] R. Zangi and S. A. Rice, Phys. Rev. E **61**, 660 (2000).
[12] A. Fortini and M. Dijkstra, J. Phys. Condens. Matter **18**, L371 (2006).
[13] M. Kahn, J.-J. Weis, C. N. Likos, and G. Kahl, Soft Matter **5**, 2852 (2009).
[14] D. H. VanWinkle and C. A. Murray, Phys. Rev. A **34**, 562 (1986).
[15] A. B. Fontecha, H. J. Schöpe, H. König, T. Palberg, R. Messina, and H. Löwen, J. Phys. Condens. Matter **17**, S2779 (2005).
[16] E. C. Oğuz, A. Reinmüller, H. J. Schöpe, T. Palberg, R. Messina, and H. Löwen, J. Phys. Condens. Matter **24**, 464123 (2012).
[17] B. Liu, A. Imhof, and A. van Blaaderen, Ordered packing of colloidal particles with long-range repulsions between two parallel confining walls (to be published).
[18] S. H. Lee, E. Y. Fung, E. K. Riley, and C. M. Liddell, Langmuir **25**, 7193 (2009).
[19] E. K. Riley and C. M. Liddell, Langmuir **26**, 11648 (2010).
[20] F. C. Cheong and D. Grier, Opt. Express **18**, 6555 (2010).
[21] D. Mukhija and M. J. Solomon, J. Colloid Interface Sci. **314**, 98 (2007).
[22] B. Liu, T. H. Besseling, M. Hermes, A. F. Demirörs, A. Imhof, and A. van Blaaderen, Nat. Commun. **5**, 3092 (2014).
[23] T. H. Besseling, M. Hermes, A. Kuijk, B. de Nijs, T.-S. Deng, M. Dijkstra, A. Imhof, and A. van Blaaderen, J. Phys. Condens. Matter **27**, 194109 (2015).
[24] A. Kuijk, A. van Blaaderen, and A. Imhof, J. Am. Chem. Soc. **133**, 2346 (2011).
[25] A. Kuijk, A. Imhof, M. H. W. Verkuijlen, T. H. Besseling, E. R. H. van Eck, and A. van Blaaderen, Part. Part. Syst. Charact. **31**, 706 (2014).
[26] See Supplemental Material at http://link.aps.org/supplemental/10.1103/PhysRevLett.115.078301 for movies and details of the experiments, the analysis, and the model calculations, which includes Ref. [27–34].
[27] S. H. Behrens and D. G. Grier, Phys. Rev. E **64**, 050401 (2001).
[28] A. Yethiraj and A. van Blaaderen, Nature (London) **421**, 513 (2003).
[29] G. J. Jan and S. S. Danyluk, Chem. Rev. **60**, 209 (1960).
[30] S. Rodríguez, C. Lafuente, P. Cea, F. M. Royo, and J. S. Urieta, J. Chem. Eng. Data **42**, 1285 (1997).
[31] T. H. Besseling, J. Jose, and A. van Blaaderen, J. Microsc. **257**, 142 (2015).
[32] T. Savin and P. S. Doyle, Biophys. J. **88**, 623 (2005).
[33] E. Eggen, M. Dijkstra, and R. van Roij, Phys. Rev. E **79**, 041401 (2009).
[34] J. N. Israelachvili, Intermolecular and Surface Forces (Academic Press, Waltham, MA, 2011).
[35] D. L. J. Vossen, M. J. A. de Dood, T. van Dillen, T. Zijlstra, E. van der Drift, A. Polman, and A. van Blaaderen, Adv. Mater. **12**, 1434 (2000).
[36] D. Frenkel and B. M. Mulder, Mol. Phys. **55**, 1171 (1985).
[37] J. Schneider, W. Hess, and R. Klein, J. Phys. A **18**, 1221 (1985).
[38] J. Schneider, W. Hess, and R. Klein, Macromolecules **19**, 1729 (1986).
[39] T. Kirchhoff, H. Löwen, and R. Klein, Phys. Rev. E **53**, 5011 (1996).
[40] K. M. Ryan, A. Mastroianni, K. A. Stancil, H. Liu, and A. P. Alivisatos, Nano Lett. **6**, 1479 (2006).
[41] J. L. Baker, A. Widmer-Cooper, M. F. Toney, P. L. Geissler, and A. P. Alivisatos, Nano Lett. **10**, 195 (2010).
[42] S. Ahmed and K. M. Ryan, Nano Lett. **7**, 2480 (2007).
[43] T. Deng et al. (to be published).